Electronic Supplementary Material (ESI) for Chemical Communications.
This journal is © The Royal Society of Chemistry 2015

Supporting Information

Light-Cleavable Rapamycin Dimer as a Universal Optical Trigger for Protein Dimerization

Kalyn A. Brown,[a,b] Yan Zou,[b] David Shirvanyants,[c] Jie Zhang,[b] Subhas Samanta,[a] Pavan K. Mantravadi,[a] Nikolay V. Dokholyan[c] and Alexander Deiters*[a,b]

[a]University of Pittsburgh, Department of Chemistry, Pittsburgh, PA 15260; [b]North Carolina State University, Department of Chemistry, Raleigh, NC 27695-8204; [c]University of North Carolina, Department of Biochemistry and Biophysics, Chapel Hill, NC 27599

SMALL MOLECULE SYNTHESIS

The synthetic scheme is shown in **Supporting Figure S1** and the NMR spectra of new compounds are shown in **Supporting Figures S2-S3**. In short, rapamycin was acylated with the *N*-succinimidyl carbonate **1**[1] according to a literature procedure that enables selective modification of the C40 position,[2] yielding the caged rapamycin monomer **2** in 45% yield. This yield is comparable to other reported modifications of rapamycin.[3,4] The tethered triple bond in **2** was then used in a highly efficient double [3+2] cycloaddition reaction with 1,4-diazidobutane in the presence of $CuSO_4$, sodium ascorbate, and tris[(1-benzyl-1*H*-1,2,3-triazol-4-yl)methyl]amine (TBTA),[5] delivering the rapamycin dimer **dRap** in 85% yield.

General synthesis methods. Reactions were performed under nitrogen using flame-dried glassware. CH_2Cl_2 was dried by a MB SPS Compact solvent purification system and stored over 4 Å molecular sieve. All other reagents and solvents were used without further purification. Spectra were recorded in $CDCl_3$, and chemical shifts are reported relative to $CHCl_3$ (7.24 ppm for ^{1}H NMR).

1-(5-Methoxy-2-nitro-4-prop-2-ynyloxyphenyl) ethanol-caged rapamycin (2). In a flame-dried vial, rapamycin (**Rap**) (50.0 mg, 0.055 mmol) was dissolved in dry DCM (1.3 ml) under argon. DMAP (13.4 mg, 0.109 mmol) and 1-(5-methoxy-2-nitro-4-prop-2-ynyloxyphenyl)ethyl *N*-succinimidyl carbonate[1] (**1**, 107.0 mg, 0.273 mmol) were added. The reaction mixture was stirred at room temperature for 20 h, the solvent was evaporated under reduced pressure, and the product was purified by column chromatography on SiO_2 (eluted with DCM/ethyl acetate 10:1, 5:1, 2:1, 1:1), delivering 29.2 mg (45% yield) of **2** as a light yellow solid. ^{1}H NMR (300 MHz, $CDCl_3$) δ 7.75 (s, br, 1H), 7.07 (d, 1H), 6.36-6.21 (m, 3H), 6.17-6.04 (m, 1H), 5.95-5.84 (m, 1H), 5.54-5.36 (m, 2H), 5.25 (d, *J* = 5.4 Hz), 5.17-5.07 (m, 2H), 4.79-4.67 (m, 3H), 4.60-4.15 (m, 2H), 3.94 (s, 3H), 3.90-3.51 (m, 3H), 3.47-3.22 (m, 8H), 3.18-3.03 (m, 5H), 2.87-2.50 (m, 3H), 2.38-2.11 (m, 1H), 2.03-1.63 (m, 12H), 1.61-1.32 (m, 12H), 1.24-0.86 (m, 27H); MS calcd for $[M + Na]^+$ $C_{64}H_{90}N_2NaO_{19}$ 1213.60, found 1213.60.

Light-cleavable rapamycin dimer (dRap). The caged rapamycin **2** (28.1 mg, 0.0235 mmol) and 1,4-diazidobutane[6] (1.0 mg, 0.071 mmol) were dissolved in H_2O (0.5 ml), *t*-BuOH (0.5 ml) and DCM (0.5 ml). $CuSO_4$ • 5 H_2O (0.5 mg, 0.002 mmol), tris[(1-benzyl-1*H*-1,2,3-triazol-4-yl)methyl]amine (TBTA, 3.8 mg, 0.007 mmol) and sodium ascorbate (4.3 mg, 0.021 mmol) were added to the solution. The reaction mixture was heated to 40 °C for 24 h. The solvents were concentrated under reduced pressure and the resulting residue was dissolved in small amount of DCM/MeOH and purified by column chromatography on SiO_2 (eluted with 33% DCM in EtOAc, then 5% MeOH in EtOAc), delivering 15.3 mg (85% yield) of **dRap**. ^{1}H NMR (300 MHz, $CDCl_3$) δ 7.74 (s, br, 2H), 7.63 (s, br, 2H), 7.06 (d, *J* = 3.0 Hz, 2H), 6.40-6.37 (m, 6H), 6.35-6.10 (m, 2H), 5.95-5.82 (m, 2H), 5.52 (dd, *J* = 8.7 Hz and *J* = 15.3 Hz, 2H), 5.37 (d, *J* = 9.9 Hz, 2H), 5.29-5.24 (m, 6H), 5.20-5.08 (m, 2H), 4.74 (s,

2H), 4.43-4.31 (m, 6H), 4.28-4.18 (m, 2H), 3.92 (s, 6H), 3.88-3.52 (m, 8H), 3.41-3.20 (m, 18H), 3.19-3.02 (m, 10H), 2.72-2.63 (m, 4H), 2.59-2.48 (m, 2H), 2.40-2.19 (m, 4H), 1.94 (s, br, 10H), 1.83-1.62 (m, 24H), 1.58-1.30 (m, 22H), 1.17-0.65 (m, 44H). ^{13}C NMR (100MHz) δ 215.4, 208.2, 192.5, 171.1, 169.2, 166.8, 154.3, 153.7, 145.6, 140.1, 139.6, 136.2, 135.6, 134.4, 133.6, 130.2, 129.5, 126.6, 126.4, 110.3, 108.1, 98.7, 84.7, 80.6, 80.2, 77.2, 77.1, 75.4, 71.9, 67.2, 60.4, 59.3, 57.0, 56.5, 56.4, 55.9, 51.3, 49.5, 46.6, 44.2, 41.5, 40.5, 40.2, 38.9, 38.2, 35.6, 35.1, 33.8, 33.2, 32.8, 31.9, 31.2, 31.1, 29.7, 29.6, 27.2, 27.1, 25.3, 22.0, 21.5, 20.7, 16.2, 16.0, 15.9, 14.2, 14.1, 13.67, 13.2, 10.2. HRMS calcd for $[M + Na]^+$ $C_{132}H_{188}N_{10}NaO_{38}$ 2544.2984, found 2545.3106.

MOLECULAR DYNAMICS SIMULATIONS

All simulations were performed using GROMACS 4.5.5.[7] CHARMM27 force field[8] was used with explicit TIP3P (Gromacs optimized) water model. Topology and force field parameters for **Rap** and its analogs were obtained from the Swissparam server.[9] To better model physiological conditions, all systems included 0.14 M of NaCl. Simulations were conducted at a constant pressure of 1 bar and constant temperature of 300K unless otherwise mentioned. Integration time steps were 3 fs. Van der Waals and electrostatic short-range cat-offs were set at 1.2 nm, and long-range electrostatics were treated by PME engine. Simulations were conducted in dodecahedron-shaped box. Box size was selected to have periodic images of the largest molecule separated by at least double of its size. Specifically, when the largest molecule is the FKBP12 protein (size is ~2.5 nm), the box size was 8 nm. In presence of **dRap** (average distance between rings ~4nm), the box size was 12 nm.

For each system, at least 10 trajectories were generated starting from the same initial configuration and with randomized initial velocities. Steered simulations were performed using Gromacs' center of mass (COM) pulling method with distance pull geometry. In this method, the pulling potential origin is moving along the vector connecting the centers of mass of the pulled molecules, and is not restricted to a particular orientation of the molecules.

Work of dissociation was calculated using the time-dependent pulling force and the center of mass of the pulled molecule recorded at 0.3 ps intervals. Work as a function of separation distance was calculated separately for each of the 10 trajectories by trapezoid rule numerical integration method.

The structure of the crystallized ternary complex[10] of FKBP12/rapamycin/FRB indicates that position C40 of rapamycin is not on the binding interface with either of the proteins. This observation is in agreement with existing experimental evidence, which suggests that modification of the rapamycin molecule at position C40 does not affect its ability to bind FKBP12,[11, 12, 13] FRB,[14] or form a ternary complex (pRap[2], HE-Rapa[5]). Rapamycin with a linker attached at C40 and anchored to the surface of a growing protein aggregate can bind FKBP12, which appears to deter further aggregation on that surface.[13] This observation indicates that the FKBP12 molecule can not only bind to a modified rapamycin anchored to a surface, but can inhibit protein-protein interactions, though it remains unclear whether this bound FKBP12 can itself interact with other proteins. Thus, the experimental evidence is mostly consistent with possibility of **dRap** binding to FKBP12 and FRB. However, we observe association of **dRap** with FKBP12, but not with FRB, which raises questions about the structure of the **dRap**-FKBP12 complex and its interaction with FRB.

In order to understand why **dRap** does not engage in formation of a ternary complex with FKBP12 and FRB, a series of atomistic molecular dynamics simulations were conducted. First, the model setup was benchmarked against known thermodynamics parameters of **Rap** complexes. Next, using this setup the behavior of **dRap**-based protein complexes was simulated.

Different mechanisms may lead to the experimentally observed association of **dRap** with FKBP12 but not FRB. One such mechanism could be steric hindrance of FRB binding caused by either the second **Rap** structure alone or a second bound FKBP12 protein. Another mechanism suggests that the binding mode of **dRap** to FKBP12 may be different from that of **Rap** to FKBP12, thereby preventing formation of an optimal binding interface for FRB molecules. A third mechanism may involve formation of the stable complex of **dRap** and two FKBP12 molecules, capable of outcompeting the ternary complex containing FRB.

The trivial steric hindrance due to the close proximity of the second **Rap** natural product appears to be an unlikely scenario. The linker length of **dRap** is sufficient to permit association of the FRB molecule with the **dRap**-FKBP12 complex (**Figure S5**). In principle, a stretched linker conformation may be unfavorable, but a 120 ns long simulation at an elevated temperature of 420 K revealed only a negligibly small (ΔG < 1 kBT = 3.5 kJ/mol) preference for the linker to be in a compact conformation (**Figure S8**). This difference is much smaller than the free energy of FRB association, ΔG_{FRB} = –74.2 kJ/mol (estimated from a K_D at 300 K),[14] and is insufficient to prevent FRB association.

To elucidate possible differences between the binding modes of **dRap** and **Rap** to FKBP12, a series of 10 independent 72 ns docking simulations were performed. These simulations were conducted at an elevated temperature of 420 K to accelerate pose sampling. In each simulation, a single ligand molecule was initially placed at a random site in the simulation box along with a single FKBP12 molecule. The ligand pose was sampled every 0.3 ps and compared to the experimentally[10] determined ligand pose of the FKBP12/**Rap** complex. Similarity between simulated and experimental binding poses is characterized by the root-mean-square difference (RMSD) between the positions of atoms of the ligand. This difference is determined by first aligning the structure of the simulated FKBP12 to the crystal structure[10] of FKBP12 in complex with **Rap**, followed by calculating the mean distance between ligand atoms (excluding hydrogen atoms). In the case of **dRap**, the RMSD was determined between atoms of **Rap** in the crystal structure and corresponding atoms of the rings in the simulated **dRap** molecule. RMSD was computed for both rings of **dRap** and the smallest value was selected to characterize the pose (**Figure S6**). In the simulations, the binding pose of the **Rap** molecule is very well recapitulated, while **dRap** has a different ensemble of binding poses. The difference of binding pose distributions is expected, given the different structure of the ligands. The ensemble of **dRap** binding poses contains a significant fraction of **Rap**-like binding poses, which may be sufficient to permit FRB binding. To estimate the effect of binding pose ensemble difference on the binding energy balance, the entire ensemble of **dRap** poses in the bound state was split into two sub-ensembles, denoted as “FRB-compatible” with an RMSD < 0.15 nm and “FRB-incompatible” with an RMSD > 0.15 nm. In these simulations, the fraction of FRB-compatible poses is P_{comp} = 0.15 ± 0.07 (**Figure S6**) which corresponds to an energetic barrier of ~ 6.6 kJ/mol. This energetic cost of placing **dRap** into the FRB compatible binding pose is much smaller than ΔG_{FRB} = –74.2 kJ/mol. Thus, it is unlikely that binding of **dRap** to FKBP12 is in an aberrant pose that prevents FRB association with the complex.

Finally, to test if **dRap**-mediated interaction of two FKBP12 molecules can successfully compete with the notoriously strong binding of FRB to the FKBP12-**Rap** complex, the free energies of complex formation for both systems were computationally compared. The free energies were calculated using non-equilibrium steered molecular dynamics (SMD) simulations. In these simulations, ligand and substrate are being pulled away from each other using harmonic potentials with moving origins.[15] The free energy of binding can then be estimated from the amount of work required to break the complex apart with the upper limit of free energy given by the Jarzynski equality.[16]

The important parameters of SMD simulations are the harmonic potential force constant and the origin pulling rate.[15] A high pulling rate results in more energy dissipation and overestimated free energy of binding. A large force constant reduces deviations of ligand from the pulling trajectory, but results in larger force fluctuations (**Figure S9**). In the simulations, an attempt to stay in quasi equilibrium regime was made by choosing a pulling rate such that the average force-driven displacement (0.02 nm/ns, **Figure S10**) remains small compared to the Brownian motion (diffusion coefficient of **dRap** D_c = 0.45 ± 0.06 nm^2/ns, and FKBP12 D_c = 0.32 ± 0.04 nm^2/ns).

In the SMD simulations, steering potential was applied along the vector between centers of mass of the ligand and substrate and did not dictate a specific dissociation pathway. At least 10 trajectories were generated with sufficient time to bring interacting molecules at least 1.2 nm apart, which is the cut-off distance for Van der Waals and short-range Coulomb interactions. This distance approximately corresponds to 1.5 r_D (Debye screening length, in 0.14 M NaCl r_D ~ 0.8 nm[17]) and beyond this distance long-range electrostatic interactions in the simulations contribute less than 10% to the total electrostatic energy in the system. The work of dissociation in each trajectory can then be computed by integrating instantaneous force along the ligand path (**Figure S7a**).

Table S1. Binding free energies ΔG_D, computed in simulations and estimated from measured dissociation constants (K_D). Standard error of simulated ΔG_D was calculated from 10 independent SMD runs.

	Simulated / kJ mol^{-1}	Experimental[14] / kJ mol^{-1}
FKBP12-Rap	85 ± 4	55
FKBP12-Rap-FRB	94 ± 5	75
FKBP12-dRap-FKBP12	>120	NA

Dissociation work was computed by averaging corresponding Boltzmann weights and their first moments (unweighted, arithmetic average).[15]. The unweighted average has resulted in larger estimated work of dissociation (**Figure S11**). This difference reflects the wide spectrum of ligand dissociation pathways with different work of extraction. The application of the Jarzinski's work estimator in non-equilibrium simulations is explained in more detail in the literature.[18,15] The dissociation work obtained by averaging Boltzmann weights is reported in **Table S1**. As a benchmark of this SMD-based computational approach, its predictions were compared with experimentally measured binding affinities of binary complexes. The experimental energy of binding of **Rap** to FKBP12 and to the FRB domain in conjunction with FKBP12 can be directly computed from the published dissociation constants.[14] In order to calculate the binding energies of **Rap**-mediated complexes, the available experimental structures of the ternary complex, FKBP12-**Rap**-FRB, were used.[10] In the case of the FKBP12-**Rap** complex, a pulling force was applied to the centers of mass of the FKBP12 and **Rap** molecules. For the FKBP12-**Rap**-FRB complex, the pulling force was applied to the centers of mass of the FKBP12 and FRB molecules, while leaving the rapamycin molecule unaffected.

In the case of the FKBP12-**dRap** complex, the simulations could not be initialized with an experimental structure, as it is unknown. Instead, the model of this complex was constructed from a series of equilibrium simulations at elevated temperature (T = 420 K). Ten trajectories of 120 ns each were generated starting from two FKBP12 molecules and one **dRap** molecule randomly placed into the simulation cell. System snapshots were collected every 120 ps and grouped into clusters according to the pairwise root-mean-square deviations with a cut-off of RMSD = 0.5 nm. Cluster centroid structures that were obtained were roughly grouped into different categories by the mutual orientation of the FKBP12 molecules: head-to-head, head-to-back and back-to back, **Figure S7b**. Centroids of the three most populated clusters were used to initialize pulling simulations and to compute binding energies. The first cluster centroid, belonging to the head-to-head group, resulted in the largest absolute binding energy, suggesting that the head-to-head configuration is the most probable structure for the FKBP12-**dRap**-FKBP12 complex. The calculated binding affinity is consistently overestimated, which is a known artifact of non-equilibrium simulations caused by undersampling of low-dissipation pathways of ligand dissociation.[18] However, the calculated binding affinity correlates well with experimental data and can be used to analyze the behavior of FKBP12 and FRB in the presence of the **Rap** analogs.

The FKBP12-**dRap** complex was not driven to complete dissociation as the FRB binding site becomes exposed at an earlier time when **dRap** is present in an extended conformation. The FKBP12 chains were pulled apart until the protein chains are fully dissociated, but before the dissociation of **dRap** from FKBP12. While a steady state of full dissociation has not been achieved, the calculated free energy of partial dissociation of the complex is already larger than the energy of full dissociation of the FKBP12-**Rap**-FRB complex (**Figure S12**). The difference between the binding free energies of FKBP12-**dRap**-FKBP12 and FKBP12-**Rap**-FRB exceeds ΔG_{dRap} > 10 kJ/mol (**Table S1**). In other words, formation of FKBP12 homodimers mediated by **dRap** is more favorable compared to formation to FKBP12-FRB heterodimers. The data cannot rule out the possibility of formation of heterotrimers, heterotetramers, or higher order oligomers. However, since at small concentrations the stability of larger aggregates is reduced compared to the stability of dimers, it appears reasonable to assume that in this system the role of heterotrimers and heterotetramers would be negligibly small. Thus, the inability of **dRap** to heterodimerize FRB and FKBP12 is likely caused by the dominating engagement of **dRap** in the formation of FKBP12 homodimers.

EXPERIMENTAL PROTOCOLS

Fluorescence Polarization Assay. FKBP12 (R&D Systems) was stirred with fluorescein isothiocyanate (FITC) at a 1:5 ratio for 3 hours in carbonate-bicarbonate buffer (pH 9.0). FKBP12-FITC was separated from free FITC by overnight dialysis (MWCO 3,500 Da; Spectrum Laboratories, Inc.) into phosphate buffered saline (PBS; pH 7.4). Protein was recovered and the concentration was determined by measuring absorbance on a NanoDrop ND-1000 spectrophotometer using the literature value for the molar extinction coefficient of FITC.[19] FKBP12-FITC was diluted to 2 μM and **dRap** was dissolved at a 100X the final concentration in PBS. FKBP12-FITC was aliquoted into a 384-well plate and **dRap** 100X stocks were added resulting in the required final concentrations of 200 nM, 2 μM, or 20 μM. After 20 minutes of incubation at room temperature, fluorescence polarization was measured on a Biotek Synergy 4 microplate reader.

K-LISA mTOR Activity Assay. GST-p70S6K (Calbiochem) was incubated in glutathione coated plates for 1 hour. mTOR (Sigma-Aldrich) was mixed with FKBP12 (R&D Systems) and either **Rap** (100 nM) or **dRap** (50 nM). Samples were placed in the dark or irradiated with UV light for 3 minutes on a transillumintor (365 nm, 25 W) and then kept on ice for 20 minutes. The samples were added to GST-p70S6K containing wells and incubated at 30 ˚C for 30 minutes. p70S6K phosphorylation was detected with an α-p70S6K-T389 phosphorylation antibody and Luminata Forte ELISA HRP Substrate (Millipore) on a Biotek Synergy 4 microplate reader.

TEVp Complementation Assay. HEK-293T cells were maintained at 37 °C and 5% CO_2 in Dulbecco's modified Eagle's medium (Hyclone) supplemented with 10% fetal bovine serum (Hyclone) and 10% streptomycin/penicillin (MP Biomedicals). Cells were passaged into a 96-well plate and when 80-90% confluent, were transfected with pFRB-TEVnt, pFKBP12-TEVct, and pTriExGloSensor (100 ng/each) using Lipofectamine 2000 (0.5 μL) (Invitrogen) according to manufacturer's protocol. Twenty-four hours after transfection **Rap** (100 nM) or **dRap** (50 nM) were added and cells were incubated for 3 hours at 37 °C and 5% CO_2. Luciferase activity was determined using a Bright Glo-Luciferase Reporter Assay kit (Promega) and a Biotek Synergy 4 microplate reader.

Cre Recombinase Complementation Assay. HEK-293T cells were passaged into two 4-well chamber slides, and grown to 80% confluency. The cells were then transfected with the Cre Stoplight (600 ng, 1 well per slide), pcDNA-FKBP-Cre59 (60 ng, 1 well per slide) and pcDNA-FRB-Cre60 (60 ng, 1 well per slide) using X-tremeGENE HP DNA transfection reagent (2:1 X-tremeGENE/DNA; Roche Biomedicals) in OptiMEM medium (Invitrogen). The transfection mixture was incubated at 37 °C for 6 hours, followed by the replacement of the OptiMEM transfection medium with DMEM. The cells were then incubated with **Rap** (10 nM) or **dRap** (5 nM) at 37 °C and 5% CO_2 overnight, followed by irradiation of selected wells for 5 min on a transilluminator (365 nm, 25 W) and replacement of medium with DMEM grow medium. Thirty-six hours post transfection, the cells were analyzed on a Carl Zeiss LSM 700 laser confocal microscope with a 20X plan-apochromat objective for the expression of GFP (excitation at 488 nm with an argon laser and emission at 493-545 nm) and DsRed (excitation at 561 nm with a solid state laser and emission at 574-659 nm) reporter proteins. Quantification of fluorescence was performed using Zen 2009 imaging software. Three independent integrations were performed.

SUPPORTING FIGURES

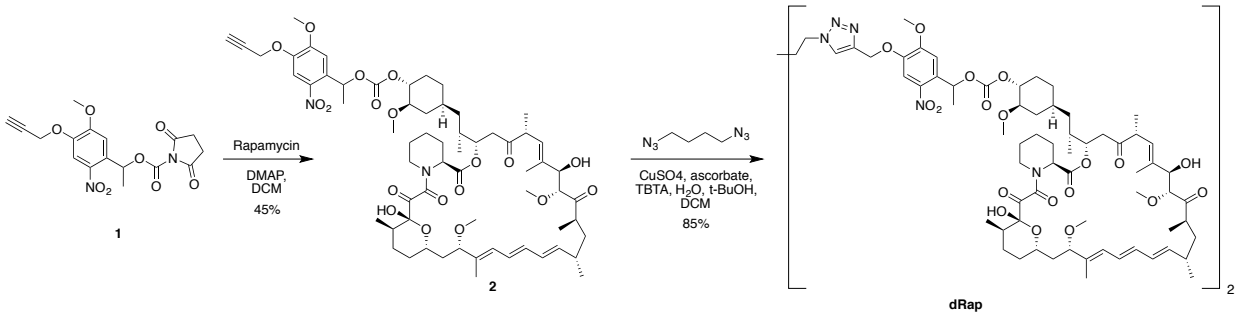

Figure S1: Synthetic reaction scheme for the light-cleavable rapamycin dimer (**dRap**).

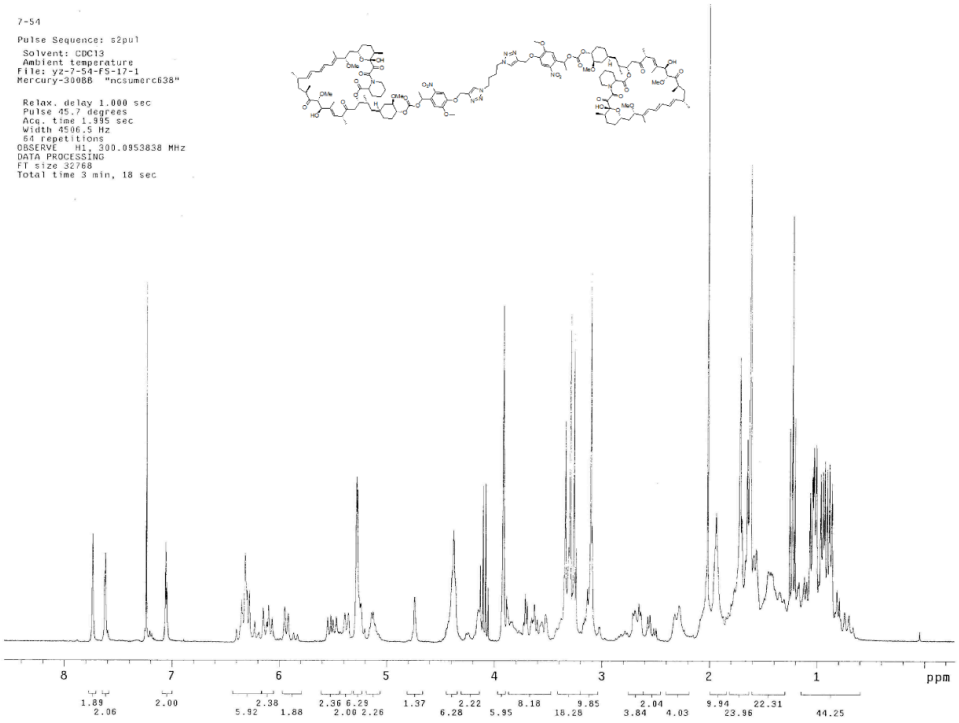

Figure S2: ^{1}H NMR spectrum of **dRap**

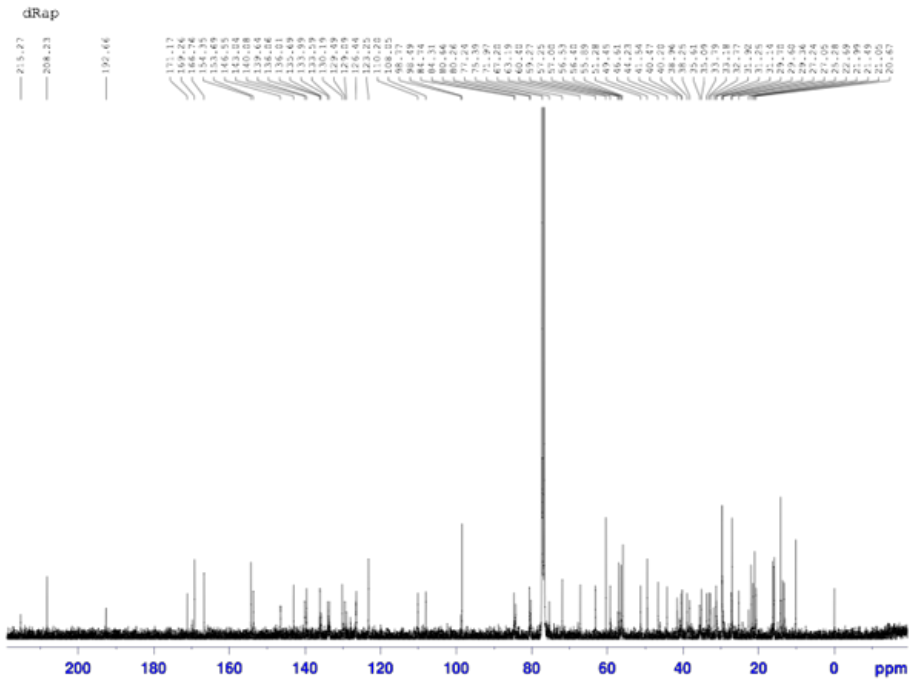

Figure S3: ^{13}C NMR spectrum of **dRap**

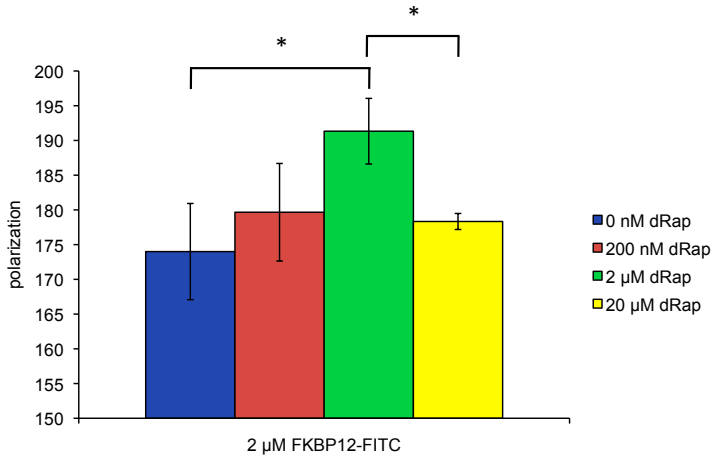

Figure S4: Fluorescence polarization of FITC labeled FKBP12 in the presence of **dRap**. Asterisks represent statistically significant differences in fluorescence polarization; P value < 0.05.

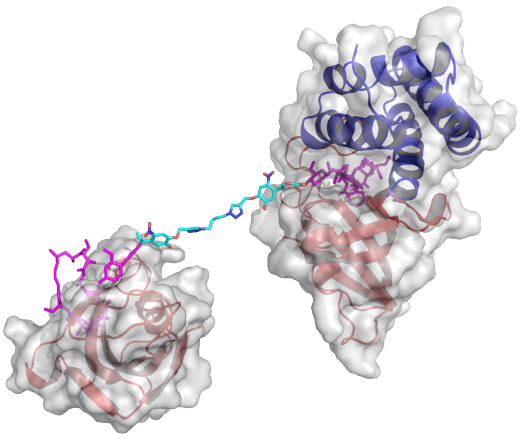

Figure S5. A hypothetical structure of the **dRap**-induced complex of FKBP12 and FRB. One copy of the FRB domain is removed for clarity. The FKBP12-FRB interface structure is based on the experimental structure of the **Rap** containing ternary complex. **Rap** is shown in pink and the light-cleavable linker (cyan) is in an extended conformation, displaying a length that is sufficient to avoid steric clashes between the two protein complexes.

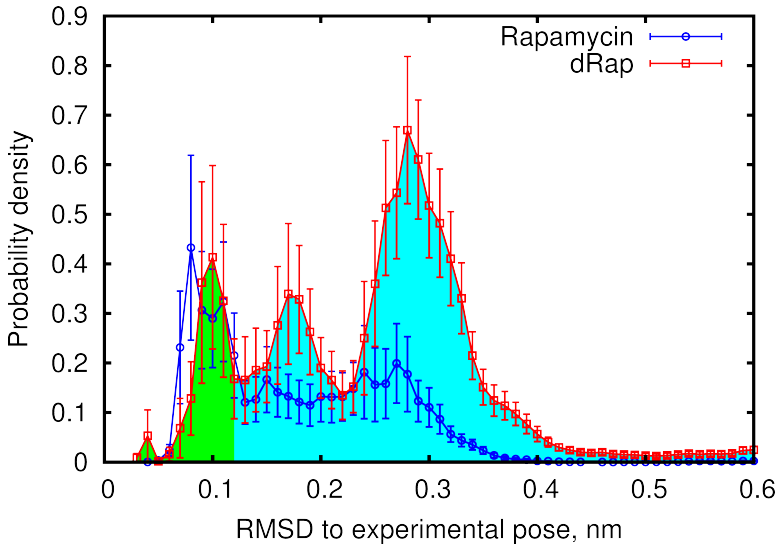

Figure S6. Distributions of root-mean-square differences of ligand atom positions between the simulated Rap binding pose and the experimentally observed[14] Rap binding pose in FKBP12. The smaller differences (RMSD < 0.15 nm) correspond to the pose that is compatible with association of the FRB domain. When the difference is large, the ligand pose may prevent interaction with FRB. For dRap, the different area fill colors mark the threshold between FRB-compatible versus FRB-incompatible poses. The estimated probability of dRap to be found in an FRB-compatible pose is $P_{comp} = 0.15 \pm 0.07$. This is a significant fraction of compatible poses and sufficient to allow heterodimerization with FRB (see discussion in the text for more detail)

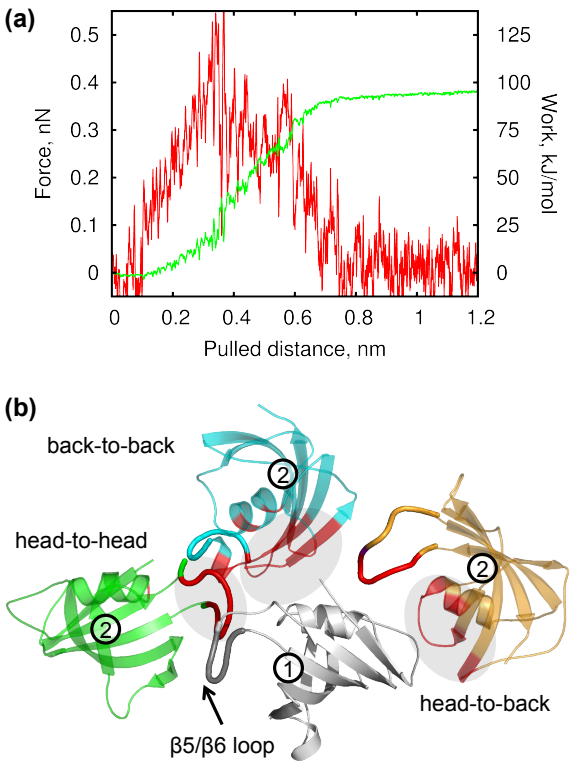

Figure S7. (a) Pulling force and work as function of pulled distance for the dual FKBP12-dRap complex starting from the head-to-head configuration. Distance is measured between centers of mass of FKBP12 chains. Force and work curves have been averaged over 10 independent simulations. (b) Typical configurations of dimer FKBP12 complexes with dRap (ligand not shown). Three representative structures have been aligned to overlay chain 1 and expose the relative orientation of chain 2. Shaded regions (marked by red color) indicate fragments of chain 2 that are in contact with chain 1. β5/β6 loop ("head") is shown with a thicker line.

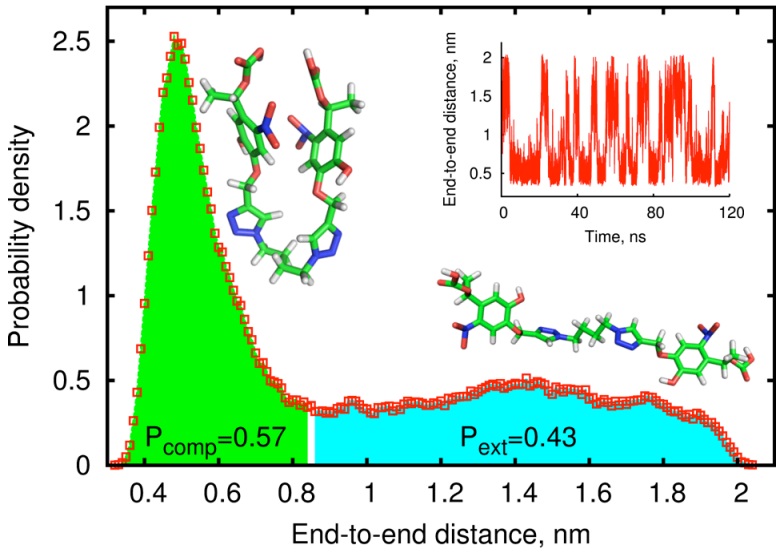

Figure S8: End-to-end distance distribution of the linker chain connecting the **Rap** fragments in the **dRap**. Inset shows distance fluctuations in the course of simulation. Multiple transitions are observed between compact and extended states.

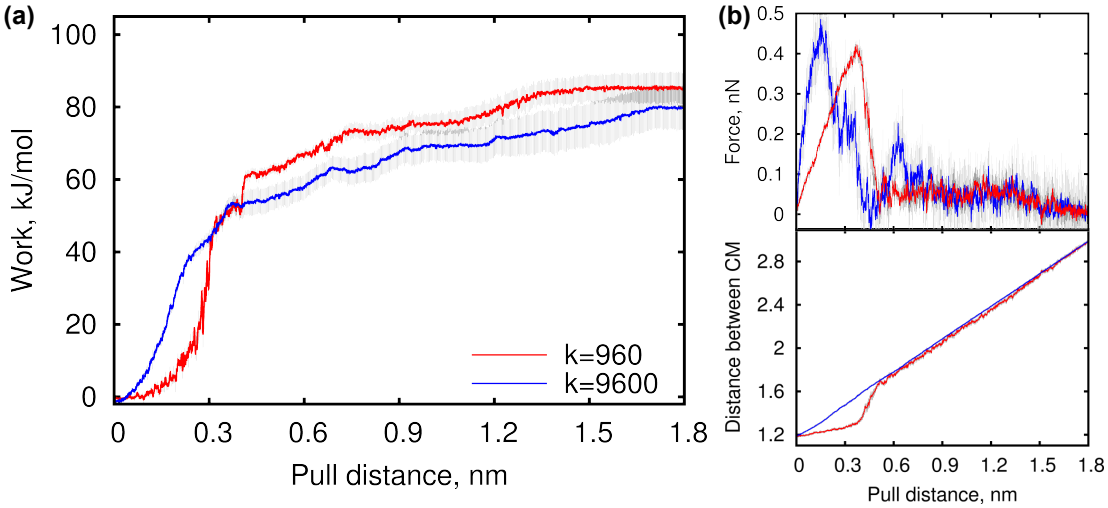

Figure S9: Steered molecular dynamics simulation of dissociation of **Rap**-FKBP12 complex performed with different force constant of the pulling potential. Changing the force constant from 960 kJ/mol/nm^2 to 9600 kJ/mol/nm^2 produces a different dissociation trajectory, but has small effect on the calculated total work of dissociation. A) Average work of dissociation as a function of position r_a of the origin of the pulling potential. B) Average force and distance between ligand and protein centers of mass. The sharp force peak indicates position of the breaking point, and softer pulling potential results in a breaking point occurring at the larger r_a ~ 0.4 nm. Shaded area indicates standard error computed over 10 trajectories. For display purposes, data curves were smoothed using running average over 150 ps window.

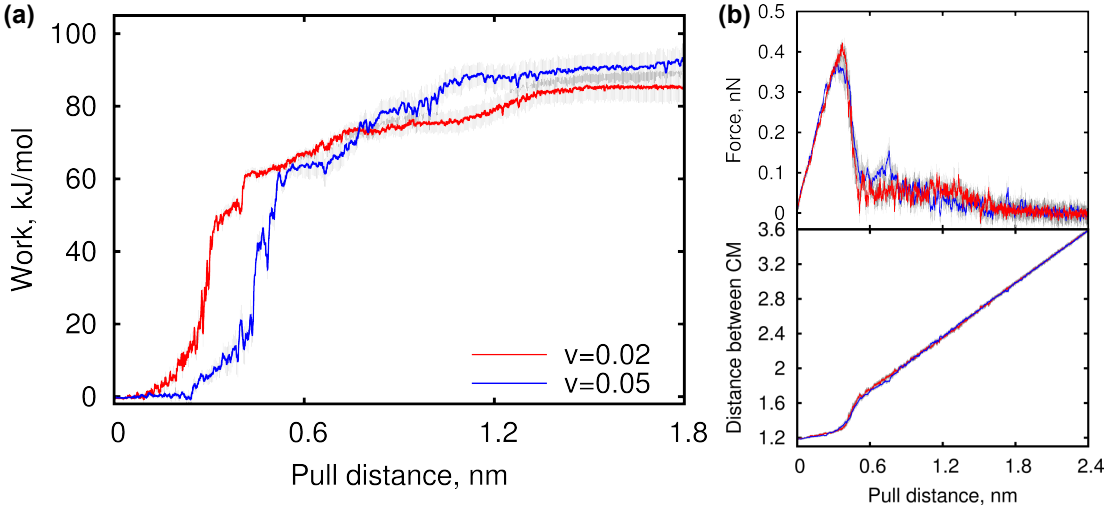

Figure S10: Steered molecular dynamics simulation of dissociation of **Rap**-FKBP12 complex performed with different pulling velocities. Changing the velocity from 0.02 nm/ns to 0.05 nm/ns produces a noticeable force spike at the position of the origin of the pulling potential r_a ~ 0.7nm. As a result the calculated total work of dissociation has increased. A) Average work of dissociation as a function of position of the origin of the pulling potential. B) Average force and distance between ligand and protein centers of mass. Shaded area indicates standard error computed over 10 trajectories. Data curves were smoothed using running average over 150 ps window.

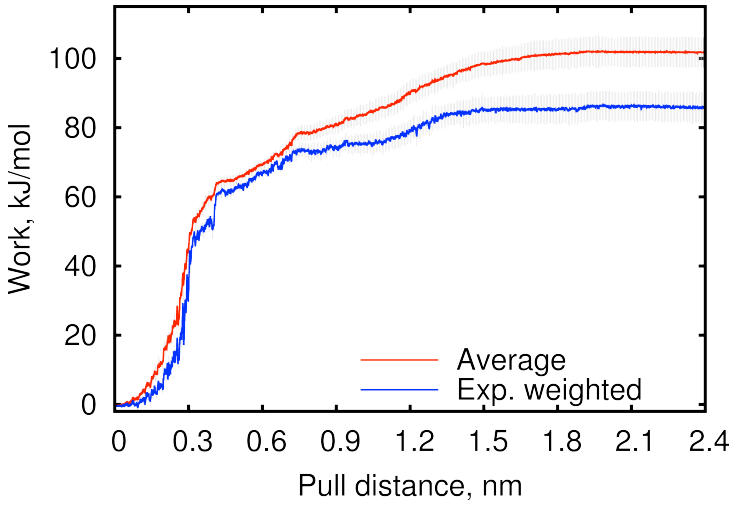

Figure S11: Unweighted average work (red curve) of dissociation of FKBP/Rap complex compared to exponentially weighted work (blue curve). The difference between weighted and unweighted work estimations at the plateau region is ~16 kJ/mol. Gray shaded area indicates standard error calculated over 10 trajectories.

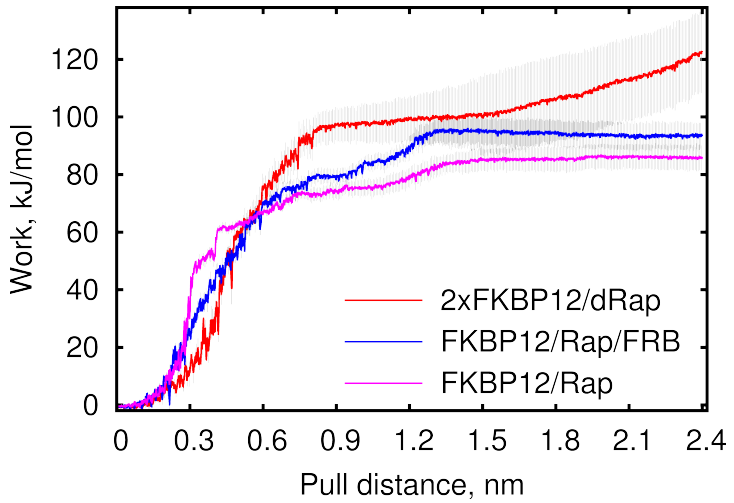

Figure S12: Work of dissociation of the **Rap** and **dRap** based complexes as a function of the pulled distance. The work of dissociation in the case of **dRap** complex does not reach plateau since pulled protein molecules are still connected by the stretched ligand and pulling work is being spent on extending the ligand linker fragment. Shaded area indicates standard error computed over 10 trajectories. Data curves were smoothed using running average over 150 ps window.

References

1. S. Kaneko, H. Nakayama, Y. Yoshino, D. Fushimi, K. Tamaguchi, Y. Horiike and J. Nakanishi, *Phys Chem Chem Phys*, 2011, **13**, 4051-4059.
2. A. V. Karginov, Y. Zou, D. Shirvanyants, P. Kota, N. V. Dokholyan, D. D. Young, K. M. Hahn and A. Deiters, *J Am Chem Soc*, 2011, **133**, 420-423.
3. L. A. Banaszynski, L. C. Chen, L. A. Maynard-Smith, A. G. L. Ooi and T. J. Wandless, *Cell*, 2006, **126**, 995-1004.
4. R. Wagner, K. W. Mollison, L. Liu, C. L. Henry, T. A. Rosenberg, N. Bamaung, N. Tu, P. E. Wiedeman, Y. Or, J. R. Luly, B. C. Lane, J. Trevillyan, Y. W. Chen, T. Fey, G. Hsieh, K. Marsh, M. Nuss, P. B. Jacobson, D. Wilcox, R. P. Carlson, G. W. Carter and S. W. Djuric, *Bioorg Med Chem Lett*, 2005, **15**, 5340-5343.
5. N. Umeda, T. Ueno, C. Pohlmeyer, T. Nagano and T. Inoue, *J Am Chem Soc*, 2011, **133**, 12-14.
6. M. E. Jung, S. Ouk, D. Yoo, C. L. Sawyers, C. Chen, C. Tran and J. Wongvipat, *J Med Chem*, 2010, **53**, 2779-2796.
7. S. Pronk, S. Páll, R. Schulz, P. Larsson, P. Bjelkmar, R. Apostolov, M. R. Shirts, J. C. Smith, P. M. Kasson, D. van der Spoel, B. Hess and E. Lindahl, *Bioinformatics*, 2013, **29**, 845-854.
8. B. R. Brooks, C. L. Brooks, A. D. Mackerell, L. Nilsson, R. J. Petrella, B. Roux, Y. Won, G. Archontis, C. Bartels, S. Boresch, A. Caflisch, L. Caves, Q. Cui, A. R. Dinner, M. Feig, S. Fischer, J. Gao, M. Hodoscek, W. Im, K. Kuczera, T. Lazaridis, J. Ma, V. Ovchinnikov, E. Paci, R. W. Pastor, C. B. Post, J. Z. Pu, M. Schaefer, B. Tidor, R. M. Venable, H. L. Woodcock, X. Wu, W. Yang, D. M. York and M. Karplus, *J Comput Chem*, 2009, **30**, 1545-1614.
9. V. Zoete, M. A. Cuendet, A. Grosdidier and O. Michielin, *J Comput Chem*, 2011, **32**, 2359-2368.
10. J. Choi, J. Chen, S. Schreiber and J. Clardy, *Science*, 1996, **273**, 239-242.
11. T. Tamura, T. Terada and A. Tanaka, *Bioconjug Chem*, 2003, **14**, 1222-1230.
12. R. Sedrani, S. Cottens, J. Kallen and W. Schuler, *Transplant Proc*, 1998, **30**, 2192-2194.
13. J. E. Gestwicki, G. R. Crabtree and I. A. Graef, *Science*, 2004, **306**, 865-869.
14. L. Banaszynski, C. Liu and T. Wandless, *J Am Chem Soc*, 2005, **127**, 4715-4721.
15. S. Park, F. Khalili-Araghi, E. Tajkhorshid and K. Schulten, *J Chem Phys*, 2003, **119**, 3559-3566.
16. C. Jarzynski, *Physical Review Letters*, 1997, **78**, 2690-2693.
17. D. P. Tieleman, P. C. Biggin, G. R. Smith and M. S. Sansom, *Q Rev Biophys*, 2001, **34**, 473-561.
18. J. Gore, F. Ritort and C. Bustamante, *Proc Natl Acad Sci USA*, 2003, **100**, 12564-12569.
19. K. Fulton, S. Jackson and A. Buckle, *Biochemistry*, 2003, **42**, 2364-2372.